Damping and Stiffness of Particulate SiC–InSn Composite

M.N. LUDWIGSON AND R.S. LAKES*
Department of Engineering Physics
Engineering Mechanics Program
University of Wisconsin – Madison
Madison, WI, 53706, USA

C.C. SWAN
Civil and Environmental Engineering Department
University of Iowa,
Iowa City, Iowa 52242

(Received June 22, 2001)
(Revised April 24, 2002)

ABSTRACT: Metal matrix composites of silicon carbide particles in indium–tin alloy were fabricated with the aim of achieving a high value of the product of stiffness and viscoelastic damping tan δ, without excess density. Stiffness and viscoelastic damping were measured over a wide range of frequency. For monodisperse 40% by volume SiC, and for hierarchical 60% by volume SiC the composite damping increased compared with the matrix at frequencies above 100 Hz. Composite shear modulus was almost a factor two greater than matrix for 40% and a factor of four greater than that of matrix for 60%. The product of stiffness and damping exceeds that of well-known materials including polymer damping layers. Hashin–Shtrikman analysis modelled the observed stiffness increase. The damping increase at higher frequency cannot be accounted for by a purely mechanical composite model; it is attributed to thermoelastic coupling and an increase in matrix dislocations during fabrication.

INTRODUCTION

STRESS AND STRAIN relations that depend on time or frequency are called viscoelastic. Viscoelastic materials are of use in the damping of vibrations to reduce fatigue in structural elements and to prevent exposure of people to excess noise and vibration. Polymer layers are commonly added to structural components which themselves have little damping. A figure of merit for the performance of damping layers is the product of stiffness (Young's modulus E or shear modulus G) and damping (tan δ; the loss tangent,

*Author to whom correspondence should be addressed. E-mail: lakes@engr.wisc.edu

0021-9983/02/19 2245–10 $10.00/0 DOI: 10.1106/002199802027291

which is proportional to the energy loss per cycle). The loss angle δ is the phase angle between stress and strain during oscillatory loading. In known viscoelastic materials, solids that combine high damping and high stiffness are not common.

In structural metals such as brass, steel, and aluminum, viscoelastic effects are usually small; tan δ is 10^{-3} or less. Large viscoelastic effects are common in solid polymers at ambient temperature; the peak loss tangent, tan δ, is from 0.1 to 1 or more. Therefore, polymer layers are commonly used to add damping to structural members. For polymers, the product E tan δ generally does not exceed 0.6 GPa; even that value can be attained only over a narrow range of temperature [1].

In view of the limitations of polymer damping materials, metals and their composites are of interest. Substantial viscoelastic response in metals is commonly but not exclusively associated with a high homologous temperature $T_H > 0.5$ in which $T_H = T/T_{\text{melting}}$, with T as the absolute temperature [2]. A high homologous temperature occurs at room temperature for elements such as cadmium, indium, lead, and tin. Eutectic In–Sn alloy, which exhibits substantial damping exceeding 0.1 at sub-audio frequency, has been previously studied in depth [3]. Synthetic ceramics, due to their high melting point, tend to exhibit relatively little damping at room temperature; however they can exhibit significant viscoelastic effects at elevated temperature [4].

Metal matrix composites (MMCs) offer attractive physical and mechanical properties such as high specific modulus, strength, and thermal stability, yet composite design with consideration of viscoelastic properties, even creep, of particulate reinforced MMCs, is not common [5]. The effect of material microstructure has been considered in the context of viscoelastic composites [6]. The best viscoelastic response (highest figure of merit E tan δ) is achieved by incorporating stiff inclusions into a compliant, high damping matrix, as opposed to high damping inclusions in a stiff matrix, or by using a Reuss laminate morphology. Particle inclusions are superior to fibers in this context, even though they provide less stiffening effect for a given volume fraction. There is not much benefit from increasing the damping of the stiff inclusions.

Since InSn has high loss with moderate stiffness ($E = 21$ GPa; $G = 7.5$ GPa; tan $\delta = 0.1$ near 1 Hz), and since it had been characterized, it was chosen as the matrix material in a previous experiment. Laminates consisting of tungsten and InSn were observed [6] to have a combination of stiffness and loss (the product E tan δ) exceeding that of well-known materials by a factor of more than 10. Although this was a successful proof of concept, the cost and density of the tungsten would be problematical in applications.

The current study uses silicon carbide particles in an InSn matrix. SiC has a high stiffness, $E = 430$ GPa, low density, $\rho = 3.2\ \text{g/cm}^3$, and reasonable cost [7]. The SiC constituent provides the strong, stiff inclusions, while the InSn provides the high damping, moderately compliant matrix. One concern is the bonding of the two constituents. A SiC–Sn composite was attempted but abandoned since it was found Sn does not wet SiC: the molten matrix rejected the particles to the perimeter. Surface-active alloys can assist in wetting particles. InSn was considered in light of its wetting properties [8] and was chosen in view of the previous experimental results mentioned above.

The purposes of this study are to fabricate composites with particles of SiC in an InSn matrix, measure the stiffness and damping over a range of frequency, and to compare the data to predictions and to previous data for isotropic InSn. In order to achieve a high concentration of SiC, a hierarchical composite of two different-sized particles was created.

EXPERIMENTAL METHODS

Processing

SiC was chosen as the stiff reinforcement and eutectic InSn as the lossy matrix, for reasons given in the introduction. Two successful samples were produced: one of 40% by volume 0.5 mm SiC particles in an InSn matrix, the other of a hierarchy of 40% by volume 0.5 mm size SiC particles and 20% by volume 0.1 mm SiC particles in an InSn matrix.

SiC particles [9] and chunks of InSn, (99.99% metals basis, [10]) were cast in a test tube of diameter 6 mm at 220°C (InSn melts at 117°C) and mixed using a loop-shape stirring rod with the tube rotating on its side at about one cycle per second. This method prevents major agglomeration, settling, and segregation of the particles. After two minutes of stirring, the composite was tamped using a brass plug to remove porosity. The temperature was ramped at about $-2°$/s to 100°C, and the specimen was furnace cooled overnight.

For 40% by volume SiC in InSn, particles of average diameter 0.5 mm (30/40 mesh) were used. 4.719 g of InSn was combined with 1.387 g of SiC to create a mixture of 40% by volume SiC, or 22.7% by weight SiC. After casting, the rounded end was cut off using a diamond saw, to obtain a cylindrical specimen of length 34.0 mm, diameter 6.02 mm, mass 5.364 g, and density 5.54 g/cm^3. Theoretically, the density should be 5.66 g/cm^3, so porosity is about 2.4%.

For 60% by volume SiC in InSn, 2.154 g of InSn was combined with 0.945 g of 0.5 mm SiC and 0.472 g of 0.1 mm SiC (Grit 120, [11]) to create a hierarchical mixture of 60% by volume SiC, or 40% by weight SiC. After casting, the specimen was compressed with a hydraulic press to remove residual porosity. The specimen was held in a mold at 17.8 kN (4000 lb) and 90°C for 30 min. A volume decrease of 4.3% resulted. The cylindrical specimen is of length 10.58 mm, diameter 6.40 mm, mass 1.535 g, and density 4.51 g/cm^3. Theoretically, the density should be 4.81 g/cm^3, or a difference of about 6.2%. The decrease in density may be due to extrusion of some InSn which was observed around the plug during hot pressing.

Testing

Experiments were performed at ambient temperature (23–25°C) using the modified [12] broadband viscoelastic spectroscopy apparatus of Chen and Lakes [13]. This device, shown in Figure 1, was used to measure the loss angle δ and the dynamic Young's modulus and shear modulus. Each specimen was cemented with cyanoacrylate between a tungsten support rod at the fixed end and a magnet at the free end. Tungsten was used to maximize the mismatch of acoustic impedance between specimen and support rod. The purpose is to minimize parasitic damping due to wave transmission into the rod at high frequencies. Sinusoidal torque was produced electromagnetically by a Helmholtz coil acting upon the high-intensity Nd-Fe-B magnet. Angular displacement was measured via laser light reflected from a small mirror at the free end of the sample to a split-diode light detector. This technique gives tan δ data for frequencies up to about 10^5 Hz; the lower limit on frequency is dictated by the experimenters' patience. Time–temperature shifts are not used; all properties are measured directly. The method is particularly advantageous

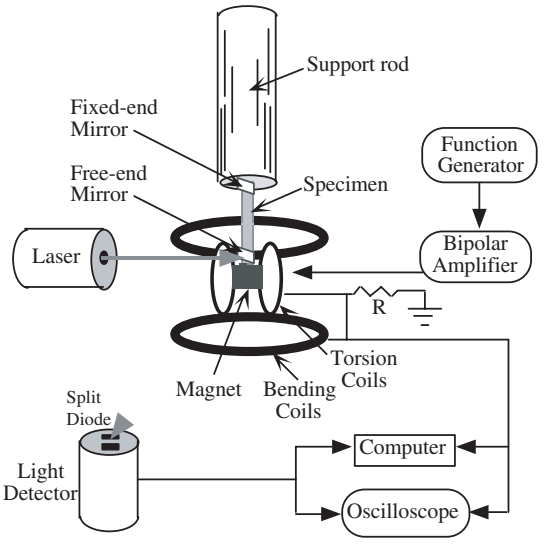

Figure 1. *Schematic diagram of the apparatus for broadband viscoelastic spectroscopy.*

for composites which, unlike amorphous polymers, do not obey time–temperature superposition. In the present study, since the emphasis is on vibration damping and sound absorption, neither very low frequency testing nor creep was done. Data were collected with LabView and a lock-in amplifier (Stanford Research SRS 850). At resonance frequencies, tan δ was inferred from the width of peaks in the dynamic compliance curve, as follows.

The damping is given by

$$\tan\delta \cong \frac{1}{\sqrt{3}}\frac{\Delta\omega}{\omega_1}, \tag{1}$$

in which ω_1 is the angular frequency at a resonance. The $\Delta\omega$ represents the full width of the resonance curve at half maximum amplitude.

The specimen stiffness was inferred from the input torque signal, the calibration of light detector and magnet, and the output voltage of the light detector. Therefore the magnet, which provides the torsion or bending moment, was calibrated on a well-characterized 6061 aluminum alloy specimen ($G = 25.9$ GPa; $\tan\delta \sim 3.6 \times 10^{-6}$). In view of the specimen thickness, stiffness, and aspect ratio, it was necessary to take precautions to prevent the compliance of portions of the system from obtruding in the data. Errors due to the compliance of the support rod and fixed end glue joint were eliminated by attaching a mirror to the fixed end of the specimen and measuring its angular displacement in a separate experiment with the same torque. If they were not eliminated by this procedure, instrumental compliance effects on the modulus would be 5.6% for torsion and 7.8% for bending. Free end glue compliance errors were eliminated by attaching the mirror to the specimen just below the magnet glue joint. Since the specimens have twice the diameter of those normally tested, a correction was applied to the resonant damping values to account for [12] the energy transmitted into the support rod.

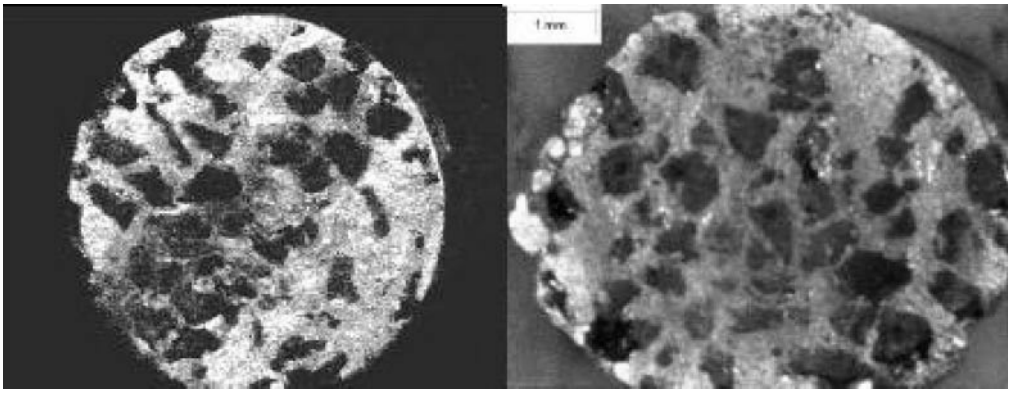

Figure 2. *Cross section views of 6 mm diameter (left) 40% SiC-InSn composite and (right) 60% SiC-InSn composite. Scale mark is 1 mm.*

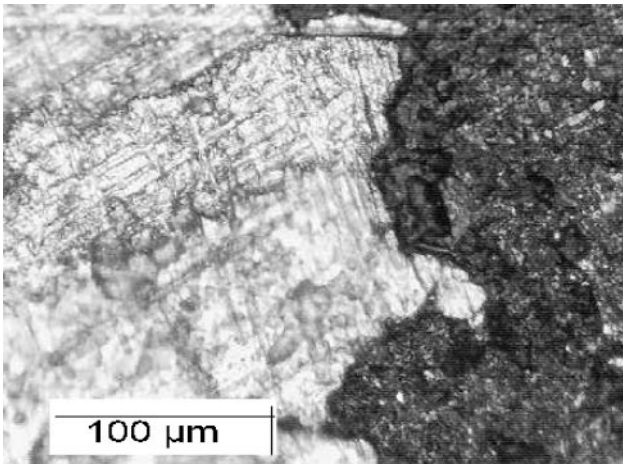

Figure 3. *A typical interface at 200× magnification between a 0.5 mm SiC particle (in black) and the InSn alloy (in white).*

RESULTS AND DISCUSSION

Figure 2 shows a cross section of the two specimens. The images suggest a reasonably random distribution of particles without agglomeration. The particles are irregular in shape. Figure 3 shows a typical interface at a higher magnification. Very few imperfections, such as gaps, were found at magnifications of 500 and 800. The composites can be considered effectively homogeneous [14], since the particles are of diameter 0.5 mm and less compared with the specimen diameter of 6.02 mm. The particles were cast randomly, therefore there was no intentional anisotropy.

We choose the Hashin–Shtrikman [15] lower formula as a model for stiffness and damping as a function of the volume fraction. Other theories [16,17], such as the composite spheres model with single size spheres, a three-phase model, the self-consistent scheme, and a concentrated suspension model give results for particulates close to the Hashin–Shtrikman lower formula.

The Hashin–Shtrikman bounding formulae apply to isotropic elastic composites. The lower bound for the shear modulus G_L of an *elastic* composite is,

$$G_L = G_2 + \frac{V_1}{1/(G_1 - G_2) + 6(K_2 + 2G_2)V_2/5(3K_2 + 4G_2)G_2} \tag{2}$$

in which K_1 and K_2, G_1 and G_2, V_1 and V_2 are the bulk moduli, shear moduli and volume fractions of phases 1 and 2, respectively. Composites obeying the Hashin–Shtrikman formulae are attained via certain hierarchical microstructures. A coated spheres structure in which the entire volume of the composite is filled with coated spheres of different size attains the Hashin–Shtrikman bounds for bulk modulus. A rank-two laminate structure [18] attains the above Hashin–Shtrikman bounds for shear modulus. In analysis of viscoelastic composites, the moduli become complex via the elastic-viscoelastic correspondence principle. The Hashin–Shtrikman formulae are no longer bounds in the viscoelastic case, but they are close to the bounds [19]. As in the elastic case, properties described by these formulae are attainable by known hierarchical microstructures. The SiC inclusions were assumed to be elastic. In view of the particulate morphology, a high volume fraction of inclusions is required to achieve composite stiffness significantly higher than that of the matrix.

The theoretical stiffness of particulate composites falls at or near the lower bound, depending on the specific morphology, assuming perfect bonding and no porosity. Based on the Hashin–Shtrikman lower formula, for a volume fraction of 40% SiC, G is 16.4 GPa. At 1 Hz, tan δ is 0.069 compared to 0.075 for InSn matrix; at 10 Hz, tan δ is 0.033 compared to 0.036 for InSn. For a volume fraction of 60% SiC, G is 26.1 GPa and tan δ is 0.063 compared to 0.075 for InSn, at 1 Hz. The predicted composite tan δ is always lower than that of the InSn alloy matrix.

The experimental shear modulus for 40% SiC was found to be a maximum of 14.2 GPa at 1000 Hz, and the dynamic elastic modulus was found to be a maximum of 25.8 GPa. Experimentally, the dynamic moduli depend on frequency since the composite is viscoelastic. The experimental shear modulus for 60% SiC was found to be a maximum of 27.4 GPa at 400 Hz, and the dynamic elastic modulus was found to be a maximum of 64.7 GPa.

The effect of residual porosity can be estimated as follows [20]:

$$E_{\text{theory}} = E_{\text{sample}}\left(\frac{\rho_{\text{theory}}}{\rho_{\text{sample}}}\right)^2 \tag{3}$$

in which E_{sample} is the stiffness of the porous sample measured experimentally, ρ_{sample} is measured to be 5.54 g/cm^3, ρ_{theory} is 5.66 g/cm^3, based on the density of inclusions and matrix and their volume fraction, assuming no porosity, and E_{theory} is the modulus if there were no porosity. This assumes spherical pores at high density, with no orientation. Therefore, porosity has the effect of reducing the modulus by 4.4% in the 40% SiC composite.

The observed composite shear moduli are close to the theoretical prediction based on the Hashin–Shtrikman lower formula, but the Young's modulus for the 40% SiC–InSn composite is less than the expected value. Modulus reduction could occur if particles agglomerated at the specimen center, but the micrographs suggest this is not the case. However, since the relatively large particles are restricted to contact with the mold walls during casting, inevitably there is a decrease in concentration at the

perimeter. Imperfect particle–matrix bonding could also account for a decrease in elastic modulus. Also, the particles as shown in Figure 2 are not spherical. Any significant elongation would make the inclusions behave in a fiber-like manner and give rise to a composite with increased modulus and reduced damping. In prior studies, the transition occurs at aspect ratios of 100 or more [21,22]. Most of the particles in Figure 2 have an aspect ratio close to 1. Therefore the effects of inclusion aspect ratio are considered minimal in this study.

The tan δ and normalized shear modulus in torsion of 40 and 60% SiC–InSn composites and the InSn alloy [3] used as a matrix are plotted in Figure 4. The tan δ inferred from creep of InSn was calculated as follows. The exact relationship for a power-law creep function, $J(t) = At^n$, is $\delta = n\pi/2$. For an arbitrary creep function a power-law may be fitted for a particular value of time. The loss tangent obtained is then an approximation. The experimental results for InSn creep follow a power-law for several decades of time, therefore the quality of the approximation is good. This is confirmed by the overlap of observed low frequency damping and values derived from creep. Composite damping properties in bending were similar to those in torsion. Also shown for comparison are the predicted modulus and damping based on a Hashin–Shtrikman model. The SiC inclusions have the favorable effect of increasing the stiffness of the composite in comparison with the matrix. An unexpected benefit is an increase in tan δ at the higher frequencies (above 100 Hz), in contrast to the decrease in damping predicted by a purely mechanical composite model. At lower frequencies (below 1 Hz), the damping of matrix and composite is similar, with somewhat lower damping in the 60% specimen at lower frequencies. At higher frequencies (above 100 Hz), the composite damping exceeds that of the matrix and the difference increases with frequency. Above 1 kHz, the tan δ of 60% SiC composite increased compared to the InSn alloy and compared to 40% SiC–InSn composite.

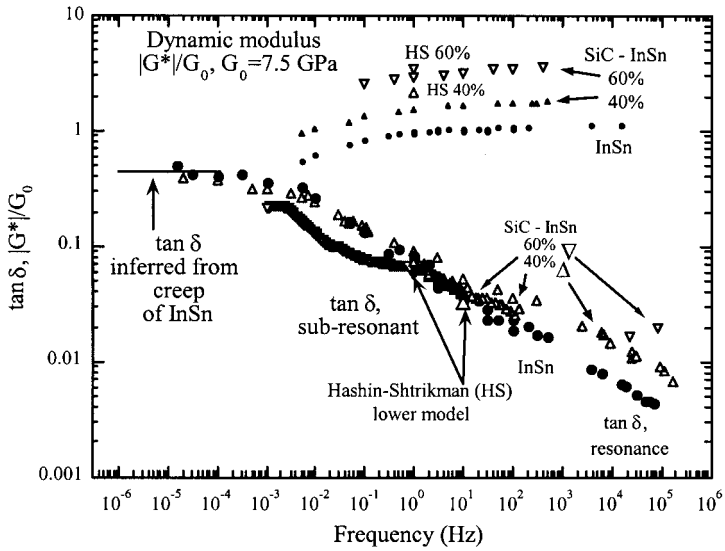

Figure 4. *Torsional damping tan δ and normalized shear modulus G/G_0 vs. frequency of 40% by volume (triangles, △) and 60% by volume (inverted triangles, ▽) SiC in InSn compared to InSn [3] (solid circles, ●). $G_0 = 7.5$ GPa. Properties were measured directly with no appeal to time temperature superposition.*

The observed high frequency increase in tan δ in the composites may be caused by several mechanisms not accounted for in the composite theory, which assumes a purely mechanical apposition of the constituents. For example, residual stress due to shrinkage as cast composites are cooled can generate dislocations in the metal matrix. A high dislocation density is known in SiC–Al composites; dislocations in the matrix elevate the composite strength [23]. These dislocations can be responsible for damping. In the present castings, differential thermal contraction during cooling is caused by the large difference in the coefficient of thermal expansion (α or CTE) of the InSn and the SiC particles. Specifically, $\alpha = 5.4 \times 10^{-6}\,\mathrm{K}^{-1}$ for SiC. Although expansion values for InSn are not available, an average value $\alpha = 27 \times 10^{-6}\,\mathrm{K}^{-1}$ for InSn may be considered based on $20 \times 10^{-6}\,\mathrm{K}^{-1}$ for Sn, $33 \times 10^{-6}\,\mathrm{K}^{-1}$ for In. It is also possible that interfaces with the particles could refine the microstructure of the eutectic alloy and give rise to enhanced damping at selected frequencies. Dislocations have been presumed to lead to the ν^{-n} dependence of tan δ in InSn and in other alloys, over many decades of frequency ν [3] following a dislocation point-defect mechanism.

Thermoelastic effects [24,25] can also contribute to the damping of composites [26–28] as well as in objects such as bent bars, in which the strain field is heterogeneous. Thermoelastic damping due to stress-induced heat flow has a characteristic frequency ν_0,

$$\nu_0 = \frac{\pi}{2}\frac{k}{C_v}\frac{1}{d^2}, \tag{4}$$

with d as thickness, k as the thermal conductivity and C_v as the heat capacity per unit volume. This is for a vibrating reed. For a one-dimensional composite inclusion of thickness d, the same relation is obtained. For a general composite, the multiplicative coefficient may differ, depending on the specific morphology. Thermal properties for InSn are not available. For Sn, with thickness 0.5 mm, $\nu_0 = 2.3$ kHz; for In, 83 Hz, and for SiC, 131 Hz. The peaks predicted are not symmetric: they remain relatively high on the high frequency end. The predicted thermoelastic peak tan δ for SiC in In is 0.004 and for SiC in Sn it is 0.014, assuming a one-dimensional model [28]. For spherical inclusions, damping will be lower [27], perhaps by a factor of two depending on the material. A further complication is the irregular shape of the particles in the present composites. Thermoelastic damping may contribute to damping at high frequencies in these composites, but dislocation damping is considered more significant.

For the 60% composite, the figure of merit E tan δ is 1.3 GPa at 100 Hz, and 5.2 GPa near 1 Hz. This figure of merit is significantly higher than the maximum, about 0.6 GPa observed in common materials (illustrated by the diagonal line in Figure 5). Polymer damping layers generally do not exceed E tan $\delta = 0.6$ GPa. Even better performance is possible if one were to incorporate a third level of structural hierarchy [29] to achieve higher volume fractions of particles. Indeed, the W–InSn laminates considered previously had E tan $\delta = 8$ GPa at 1 Hz; an optimal volume fraction (95% by volume tungsten) was obtained straightforwardly in this case by choice of layer thickness. Such high volume fractions are the due to the fact the Reuss and the Hashin–Shtrikman lower morphologies are inefficient in achieving high stiffness for given volume fraction. Nevertheless, these morphologies are of interest in damping layers since they give rise to the highest values of E tan δ for given constituent properties [6].

As for future developments in high damping composites, the optimal matrix would be stiffer than InSn since that would permit smaller volume fractions of inclusions. Since

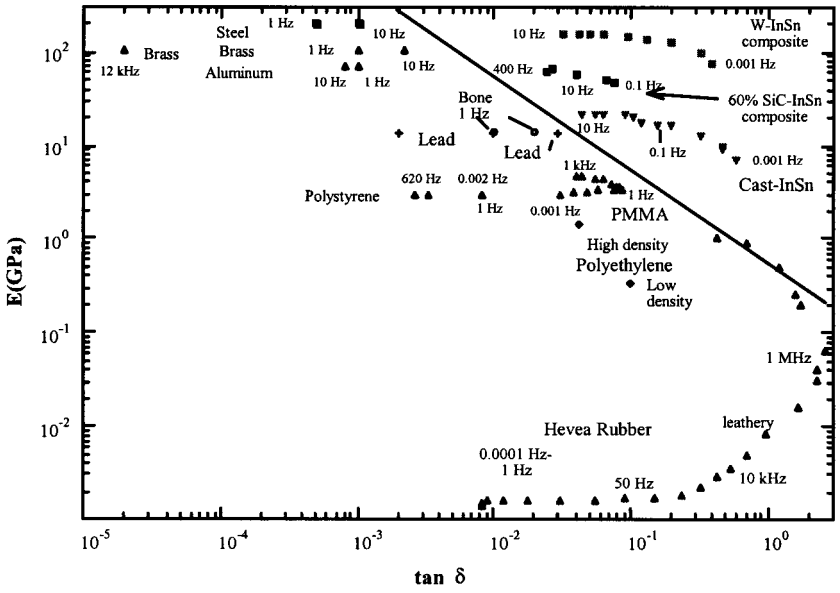

Figure 5. *Stiffness-loss map, comparing properties of several materials adapted from Lakes [30], including the present composites.*

indium is relatively expensive, a matrix containing other materials would be more desirable in terms of cost.

CONCLUSIONS

The viscoelastic damping and shear and Young's moduli were increased significantly by the addition of silicon carbide inclusions in the indium–tin alloy. Hashin–Shtrikman analysis, which assumes a purely mechanical effect of the inclusions cannot explain the increase in damping observed at high frequencies. Thermoelastic damping as well as damping due to dislocations from differential shrinkage are contributory causal mechanisms. The product of stiffness and damping exceeds that of well-known materials including polymer damping layers.

ACKNOWLEDGMENT

The authors are grateful for a grant, CMS-9896284, from NSF and for the NSF-REU program. We thank T. Lee and Y. C. Wang for assistance with the lock-in amplifier.

REFERENCES

1. Capps, R.N. and Beumel, L.L. (1990). Dynamic Mechanical Testing, Application of Polymer Development to Constrained Layer Damping. In: Corsaro, R.D. and Sperling, L.H. (eds.), *Sound and Vibration Damping with Polymers*, American Chemical Society, Washington DC.
2. Quackenbush, J., Brodt, M. and Lakes, R.S. (1996). Viscoelastic Behavior Over a Wide Range of Time and Frequency in Tin Alloys: SnCd and SnSb, *Scripta Metallurgica*, **35**: 441–447.

3. Lakes, R.S. and Quakenbush, J. (1996). Viscoelastic Behavior in Indium–Tin Alloys Over a Wide Range of Frequency and Time, *Philosophical Magazine Letters*, **74**: 227–232.
4. Wolfenden, A. (1997). Measurement and Analysis of Elastic and Anelastic Properties of Alumina and Silicon Carbide, *Journal of Materials Science*, **32**: 2275–2282.
5. Ibrahim, I.A., Mohamed, F.A. and Lavernia, E.J. (1991). Particulate Reinforced Metal Matrix Composites – a Review, *Journal of Materials Science*, **26**: 1137–1156.
6. Brodt, M. and Lakes, R.S. (1994). Composite Materials Which Exhibit High Stiffness and High Damping, *Journal of Composite Materials*, **29**: 1823–1833.
7. Buhl, H. (1992). *Advanced Aerospace Materials*, Springer-Verlag, Berlin.
8. Delannay, F., Froyen, L. and Deruyttere, A. (1987). The Wetting of Solids by Molten Metals and its Relation to the Preparation of Metal-Matrix Composites, *Journal of Materials Science*, **22**: 1–16.
9. United Abrasive, 19100 Industrial Park Drive P.O. Box 98, Vulcan, MI.
10. Alfa Aesar, High Purity Metals, pg. 251, stock #18159.
11. Buehler, 41 Waukegan Rd, Lake Bluff, IL 60044. No. 40-6400-120-016.
12. Brodt, M., Cook, L.S. and Lakes, R.S. (1995). Apparatus for Measuring Viscoelastic Properties Over Ten Decades: Refinements, *Review of Scientific Instruments*, **66**(11): 5292–5297.
13. Chen, C.P. and Lakes, R.S. (1989). Apparatus for Determining the Viscoelastic Properties of Materials Over Ten Decades of Frequency and Time, *Journal of Rheology*, **33**: 1231–1249.
14. Christensen, R.M. (1979). *Mechanics of Composite Materials*, John Wiley & Sons, Inc., New York
15. Hashin, Z. and Shtrikman, S. (1963). A Variational Approach to the Theory of the Elastic Behavior of Multiphase Materials, *J. Mech. Phys. Solids*, **11**: 127–140.
16. Tandon, G.P. and Wang, G.J. (1986). *Composite Science Technology*, **27**: 111.
17. Aboudi, J. (1991). *Mechanics of Composite Materials*, Elsevier Science Publishers B.V., Amsterdam.
18. Milton, G.W. (1986). Modelling the Properties of Composites by Laminates. In: Erickson, J.L., Kinderlehrer, D., Kohn, R. and Lions, J.L. (eds.), *Homogenization and Effective Moduli of Materials and Media*, pp. 150–175, Springer Verlag, Berlin.
19. Gibiansky, L.V. and Lakes, R.S. (1993). Bounds on the Complex Bulk Modulus of a Two-phase Viscoelastic Composite with Arbitrary Volume Fractions of the Components, *Mechanics of Materials*, **16**: 317–331.
20. Gibson, L.J. and Ashby, M.F. (1997). *Cellular Solids*, Cambridge University Press, Cambridge.
21. White, R.G. and Palmer, T.A. (1984). Control of the Properties of Carbon Fiber Reinforced Plastics, *AIAA Journal*, **22**: 1662–1669.
22. Suarez, S.A., Gibson, R.F., Sun, C.T. and Chaturvedi, S.K. (1986). The Influence of Fiber Length and Fiber Orientation on Damping and Stiffness of Polymer Composite Materials, *Experimental Mechanics*, **26**: 175–184.
23. Arsenault, R.J. and Fisher, R.M. (1983). Microstructure of Fiber and Particulate SiC in 6061 Al Composites, *Scripta Metall et Mater.*, **17**: 67–71.
24. Zener, C. (1937). Internal Friction in Solids I – Theory of Internal Friction in Reeds, *Phys. Rev.*, **52**: 230–235.
25. Zener, C. (1938). Internal Friction in Solids II. General Theory of Thermoelastic Internal Friction, *Phys. Rev.*, **53**: 90–99.
26. Bishop, J.E. and Kinra, V.K. (1994). Elastothermodynamic Damping in Composite Materials, *Mechanics of Composite Materials and Structures*, **1**: 75–93.
27. Bishop, J.E. and Kinra, V.K. (1995). Analysis of Elastothermodynamic Damping in Particle-reinforced Metal-Matrix Composites, *Metall. and Materials Trans.*, **26A**: 2773–2783.
28. Milligan, K.B. and Kinra, V.K. (1993). On the Thermoelastic Damping of a One-Dimensional Inclusion in a Uniaxial Bar, *Mechanics Research Communications*, **20**: 137–142.
29. Lakes, R.S. (2002). High Damping Composite Materials: Effect of Structural Hierarchy, *Journal of Composite Materials*, **36**: 287–298.
30. Lakes, R.S. (1998). *Viscoelastic Solids*, CRC Press, Boca Raton, FL.